Non-destructive measurement of two-dimensional refractive index profiles by deflectometry*

Di Lin, James R. Leger
Department of Electrical and Computer Engineering, University of Minnesota, 200 Union St NE, Minneapolis, MN, USA 55455

ABSTRACT

We present a method for calculating a two-dimensional refractive index field from measured boundary values of beam position and slope. By initially ignoring the dependence of beam trajectories on the index field and using cubic polynomials to approximate these trajectories, we show that the inverse problem can be reduced to set of linear algebraic equations and solved using a numerical algorithm suited for inverting sparse, ill-conditioned linear systems. The beam trajectories are subsequently corrected using an iterative ray trace procedure so that they are consistent with the ray equation inside the calculated index field. We demonstrate the efficacy of our method through computer simulation, where a hypothetical test index field is reconstructed on a 15×15 discrete grid using 800 interrogating rays and refractive index errors (RMS) less than 0.5% of the total index range ($n_{max} - n_{min}$) are achieved. In the subsequent error analysis, we identify three primary sources of error contributing to the reconstruction of the index field and assess the importance of data redundancy. The principles developed in our approach are fully extendable to three-dimensional index fields as well as more complex geometries.

Keywords: geometrical optics, inhomogeneous media, gradient-index, refractive index, deflectometry, metrology

1. INTRODUCTION

The subject of gradient-index (GRIN) optics pertains to the study of inhomogeneous optical media whose refractive index varies with position and dates back to the 1850s. For many years, the manufacturing capabilities of GRIN materials have been the primary limiting factor to successfully implementing GRIN elements in integrated optical systems. However, there are now many different material systems (primarily glasses and plastics) in which gradients in the refractive index can be made. Myriad techniques have been studied for fabricating increasingly complex index variations[1,2]. Current methods for fabricating GRIN materials include neutron irradiation[3], chemical vapor deposition (CVD)[4], ion exchange[5,6], ion stuffing[7], and variations of polymer-based processes[8-10]. The underlying physical principles behind these fabrication methods have always limited their ability to produce arbitrary index profiles. Specifically, these limitations include: (1) The physical depth into which the material's refractive index can be changed; (2) the maximum change that can be achieved in the refractive index; and (3) the types of refractive index variations that can be manufactured. However, several new methods have been developed that permit unprecedented control over the index profile in two and three dimensions[11]. Given the various technological advances in GRIN fabrication techniques we have just listed, it is reasonable to speculate that arbitrary index distributions in GRIN optical components may be realizable in the near future.

In response to these technological advances in GRIN fabrication over the last three decades, there has been increasing interest in exploring novel GRIN materials to develop compact, lightweight and robust optics. GRIN optics offer appealing form factors as well as additional degrees of freedom in controlling the propagation of light and have found application in telecommunications and compact imaging. In the former application, a refractive index profile that varies

* This review paper contains work that has previously been submitted and is scheduled for publication in J. Opt. Soc. Am. A (2015).

Modeling Aspects in Optical Metrology V, edited by Bernd Bodermann, Karsten Frenner, Richard M. Silver,
Proc. of SPIE Vol. 9526, 95260Q · © 2015 SPIE · CCC code: 0277-786X/15/$18 · doi: 10.1117/12.2184856

radially from the center of an optical fiber can be chosen properly so that the rays that transit the fiber are guided by refraction, rather than by total internal reflection (e.g., in step-index optical fibers). In addition, GRIN fibers can be designed so that all modes propagate with the same velocity, reducing modal dispersion and thereby increasing the bandwidth and the repeater distance of optical communication systems[1]. Furthermore, the cylindrical form factor of GRIN optics simplifies coupling between optical fibers and sources. It follows that the optical power of lenses is not only determined by their surface geometry but also by their refractive index distribution. By combining the two effects, new approaches to chromatic as well as spherical aberration correction become possible[12,13]. In addition, GRIN optics can be designed to redistribute irradiance in an optical beam and perform coherent mode conversion in beam shaping applications[14-16].

Since the refractive index of the GRIN element dictates the propagation of light inside the optical material, accurate knowledge of its index distribution is essential for integration into optical systems. Many methods for measuring one-dimensional (1-D) GRIN profiles have been described in the literature over the years and have found application in the study of diffusion properties of particles in liquids and gases outside the realm of GRIN optics. These include prism methods[17,18], moiré patterns[19,20], deflectometry methods based on either beam displacement[21,22] or deflection in beam angle[23], as well as interferometric methods[24-27]. In the case of two-dimensional (2-D) GRIN profiles, analytical solutions for deflectometry measurements have been shown for specific geometries, such as radially symmetric index profiles of optical fiber preforms[28]. In cases where symmetry cannot be exploited to reconstruct the index field, straight ray trajectories assumed in tomographic approaches enable the use of the projection slice theorem in the Fourier synthesis of the index field from interferometric data[29]. Furthermore, deflectometry principles have also been demonstrated in interrogating 2-D index fields using x-rays, where the index of materials is close to unity for the chosen wavelength[30,31]. However, reconstruction accuracy in these methods is quickly compromised under even a modest refracting index field where ray trajectories are seldom linear. In addition, the effects of Snell's law at the discontinuities along interfaces are either assumed to be negligible or not addressed at all in these methods. In contrast, our method of inversion is applicable to measurements performed at visible wavelengths (or any wavelength, in general); it allows for curved ray trajectories under steep index gradients and accounts for Snell's law along the boundary interface. As far as we know, there has been no reported method of directly inverting deflectometry measurements in reconstructing arbitrary 2-D index fields that offer these capabilities.

2. THE INVERSE PROBLEM

2.1 Linear system formulation

We will first develop the mathematical model upon which our method is based from the (simpler) context of interferometric measurements. Let us suppose that the index field in question, $n(x, y)$, can be represented on a uniform rectangular grid of discrete sample points, as shown in Fig. 1, where the integers l and k are discrete indices corresponding to the spatial variables x and y, respectively. In this discrete representation, we treat the sample values $n_{l,k}$ as the system's unknown quantities, which we will use synonymously with its degrees of freedom (DoFs). Of course, a sufficient number of sample points are required in representing $n(x, y)$ to avoid loss of information in the discrete representation of any continuous field quantity. Assuming that $n(x, y)$ is band-limited, the minimum number of sample points is associated with its space-bandwidth product[32].

For the sake of simplicity, let us assume that $n(x, y)$ is constant within each rectangular region and that its value is equal to the sample value $n_{l,k}$ located at its center, as shown in the figure. Next, suppose that we measure the absolute optical path length traveled by a probe laser beam that transits $n(x, y)$. Such a measurement can be described by a path integral of $n(x, y)$ in terms of the sampled values $n_{l,k}$ inside the index field. In the analog domain, the path integral can be written as

$$\varphi = \int_a^b ds \cdot n(x,y) \ , \tag{1}$$

where ds is the differential arc length and a and b are the end-points for the path traveled by the probe beam. Switching to a discrete representation under our crude approximation, the path integral can be expressed as the Riemann sum

$$\varphi = \sum_l \sum_k ds_{l,k} n_{l,k} \ , \tag{2}$$

where $ds_{l,k}$ is the arc length of the path segment contained within the rectangular region corresponding to $n_{l,k}$. If the path of the integral is known, then $ds_{l,k}$ is fully specified and Eq. (2) qualifies as a linear expression in $n_{l,k}$.

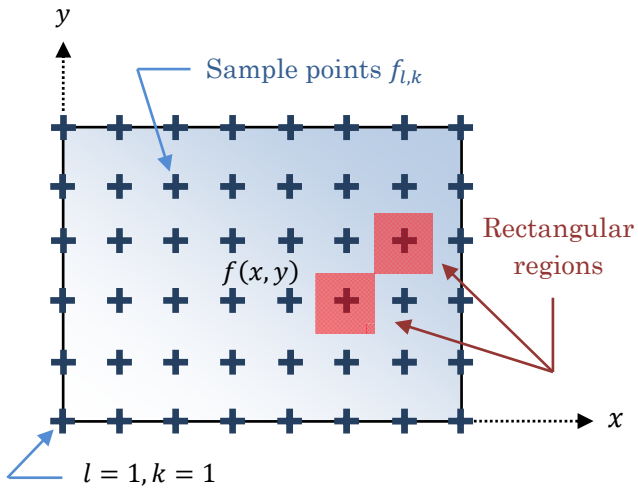

Fig. 1. Discrete representation of a continuous field quantity on a uniform rectangular grid, where values of the field are assumed to be constant within each rectangular region under a crude approximation.

2.2 Extension to deflectometry

Assuming diffraction of the probe laser beam to be negligible, the ray equation of geometrical optics[33] governs its propagation inside the index field n:

$$\frac{d}{ds}\left(n\frac{d\vec{r}}{ds}\right) = \nabla n \ , \tag{3}$$

where ds is the arc length along the ray trajectory, and $\vec{r}$ is the position of a point on the trajectory. Using small angle approximations, it is straight-forward to show from Eq. (3) that the normal component of the local index gradient induces a change in the ray's direction and that the overall angular deflection of an interrogation ray can be expressed as a path integral of the partial derivatives of the index field:

$$\Delta\theta = \int_a^b ds \cdot \nabla w \cdot \hat{t} = \int_a^b ds \cdot \left[-sin(\theta)\frac{\partial w}{\partial x} + cos(\theta)\frac{\partial w}{\partial y}\right] \ , \tag{4}$$

where $\hat{t} = -sin(\theta)\hat{\imath} + cos(\theta)\hat{\jmath}$ denotes the normal unit vector to the beam's trajectory and $\nabla w = \frac{\partial w}{\partial x}\hat{\imath} + \frac{\partial w}{\partial y}\hat{\jmath}$ is the gradient of the logarithmic index field $w = \ln(n)$. We illustrate the geometry of the deflectometry path integral in Fig. 2.

Sampling the partial derivatives $\frac{\partial w}{\partial x}$ and $\frac{\partial w}{\partial y}$ on the same rectangular grid as $n_{l,k}$ and using the crude approximation from Sec. 2.1, Eq. (4) can be rewritten as the Riemann sum

$$\Delta\theta = \sum_l \sum_k ds_{l,k} \nabla w_{l,k} \cdot \hat{n}_{l,k} \ , \tag{5}$$

where $ds_{l,k}$ is the arc length of the path segment contained within the rectangular region associated with sample values for the index gradient vector $\nabla w_{l,k}$ and $\hat{t}_{lk}$ is taken to be the mean normal unit vector for this ray segment.. As before, we assume $\nabla w_{l,k}$ to be constant within each rectangular region. Once again, we assume that the path of the integral is given so that $ds_{l,k}$ and $\hat{t}_{lk}$ are fully specified in the expression and Eq. (5) remains linear in $\nabla w_{l,k}$. Because $\frac{\partial w}{\partial x}$ and $\frac{\partial w}{\partial y}$ are the partial derivatives of the underlying potential function w, they must satisfy

$$\nabla \times \nabla w = \frac{\partial}{\partial y}\frac{\partial w}{\partial x} - \frac{\partial}{\partial x}\frac{\partial w}{\partial y} = 0 \ . \tag{6}$$

The vanishing curl in Eq. (6) ensures that $w(x, y)$ is single-valued; any gradient field ∇w with non-zero curl is unphysical. In terms of the discrete values $\nabla w_{l,k}$, Eq. (6) can be discretized as

$$\left(\left.\frac{\partial w}{\partial x}\right|_{l,k+1} - \left.\frac{\partial w}{\partial x}\right|_{l,k}\right) - \left(\left.\frac{\partial w}{\partial y}\right|_{l+1,k} - \left.\frac{\partial w}{\partial y}\right|_{l,k}\right) = 0 \tag{7}$$

and applies to all sampling grid points.

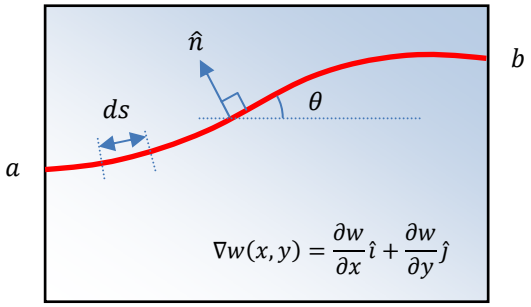

Fig. 2. Geometry of physical quantities used to describe the deflection of a probe laser beam propagating through a 2-D index field.

2.3 The system equation

Suppose that a set of probe laser beams are used to interrogate the index field in question and the boundary values of slope and position are reported for each beam. If we derive an expression for the path integral in Eq. (5) without knowledge of the laser beams' trajectories inside the index field, Eq. (5) becomes nonlinear in $\nabla w_{l,k}$ because both $ds_{l,k}$ and $\hat{t}_{lk}$ in the expression are functions of $\nabla w_{l,k}$ according to Eq. (3). In order to linearize the system, we propose to ignore the dependence of the laser beams' trajectories on the index field (and its gradient) and generate approximate trajectories based on the measured boundary values. Although the approximated trajectories are initially unphysical, we intend to use a corrective ray trace procedure to obtain trajectories that are consistent with Eq. (3) *after* obtaining an initial reconstruction of the index field.

Assimilating the Riemann sums from Eq. (5) and the irrotational constraints from Eq. (7) into a set of simultaneous linear algebraic equations results in the system equation

$$[S] \cdot \vec{\delta} = \vec{P} \ . \tag{8}$$

where the unknown vector $\vec{\delta}$ now contains sample vector components of $\nabla w_{l,k}$, half of which describes $\left.\frac{\partial w}{\partial x}\right|_{l,k}$ and the other half specifies $\left.\frac{\partial w}{\partial y}\right|_{l,k}$. Assuming we have N total measured probe beams, the first N rows of $[S]$ each contain lexicographically ordered (or raster scanned) coefficients associated with each of the unknown sample values in $\vec{\delta}$. Accordingly, the first N values in $\vec{P}$ correspond to total angular deflection values for the respective probe beams. The remaining rows of $[S]$ correspond to the irrotational constraints in the form of Eq. (7) and the respective values in $\vec{P}$ are set to zero. Assuming N is sufficient such that $[S]$ is a full-rank matrix, $[S]$ can, in principle, be inverted to solve for $\vec{\delta}$, or equivalently, the gradient vector field $\nabla w_{l,k}$. Upon integrating $\nabla w_{l,k}$, the index field is specified up to an unknown constant, which can be determined by a single independent measurement of the refractive index, e.g., along the boundary. Following the initial reconstruction of the index field, a ray trace is performed for each probe beam using the measured boundary values. The traced trajectories are then used to refine the approximate trajectories so that a new system equation can be generated (and subsequently inverted) to obtain a more accurate reconstruction. We repeat this process until the beam trajectories and the reconstructed index field are consistent with Eq. (3).

3. NUMERICAL IMPLEMENTATION

3.1 Generating deflectometry data

We began with the test index field shown in Fig. 3(a). To interrogate the medium, we applied probe beams to entry points uniformly distributed across the left and top boundary of the rectangular index field and used a numerical ray trace[34] to generate boundary values for position and external slope for all probe laser beams. The interrogating set of probe beams connect all possible pairings of entry and exit points that reside on opposite boundaries of the index field, which we illustrate for a single entry point in Fig. 3(b). Probe beams that could not be measured in the ambient medium due to total internal reflection were discarded from the simulated data.

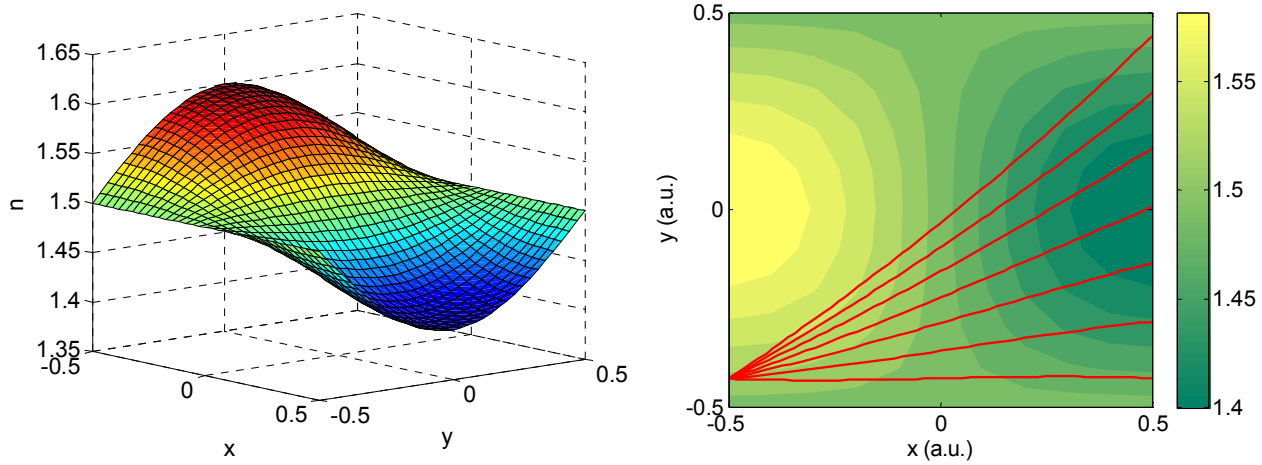

(a) (b)

Fig. 3. (a) Test index field used to generate boundary values of beam position and slope and (b) sample probe laser beams applied to a single entry point along the left boundary, connecting the entry point to all possible exit points.

Our simulated data consisted of boundary measurements for 800 interrogating probe beams, 400 of which propagate strictly between the left and right boundaries of the test index field and the other 400 between the top and bottom boundaries. The boundary beam locations and external slopes, as well as the index of refraction along the boundary

(which can be measured in practice by a refractometer, for instance), were subsequently used as input data for our recovery algorithm.

3.2 Recovering the index field

Using the boundary values of the test index field, we applied Snell's law to the generated external slope data to obtain corresponding internal slope values. We then constructed cubic polynomials from the boundary values of beam location and internal slope to approximate the trajectories for the probe beams inside the index field. From these trajectories, we used constrained cubic spline interpolation to derive a set of algebraic equations representing the deflectometry path integral in Eq. (4) corresponding to each probe beam. The resulting expressions were considerably more complex than the crude approximations used in Sec. 2.2 but were necessary to mitigate the quantization effects introduced into our deflectometry model. Augmenting these algebraic equations with the discrete irrotational constraints in Eq. (11), we arrive at a deflectometry system equation in the form of Eq. (8).

In principle, computing the inverse or the pseudo-inverse of the deflectometry system matrix $[S]$ will allow us to solve for the partial derivative fields (contained in $\vec{\delta}$) from the data vector $\vec{P}$. However, the similarity in coefficients generated by path integrals for similar probe beams makes $[S]$ inherently ill-conditioned. Furthermore, $[S]$ is sparse because only a small set of grid points pertain to individual path integrals. To address these numerical issues, we employed the method of least squares QR factorization (LSQR) to solve for $\vec{\delta}$, an iterative inversion technique that has been shown to produce reliable results in inverting sparse and ill-conditioned linear systems[35]. The resulting gradient field $\nabla w_{l,k}$ obtained from the inversion is depicted in Fig. 4(a), which was subsequently integrated to reconstruct the index field shown in Fig. 4(b), where the integration constant was determined from known boundary index values.

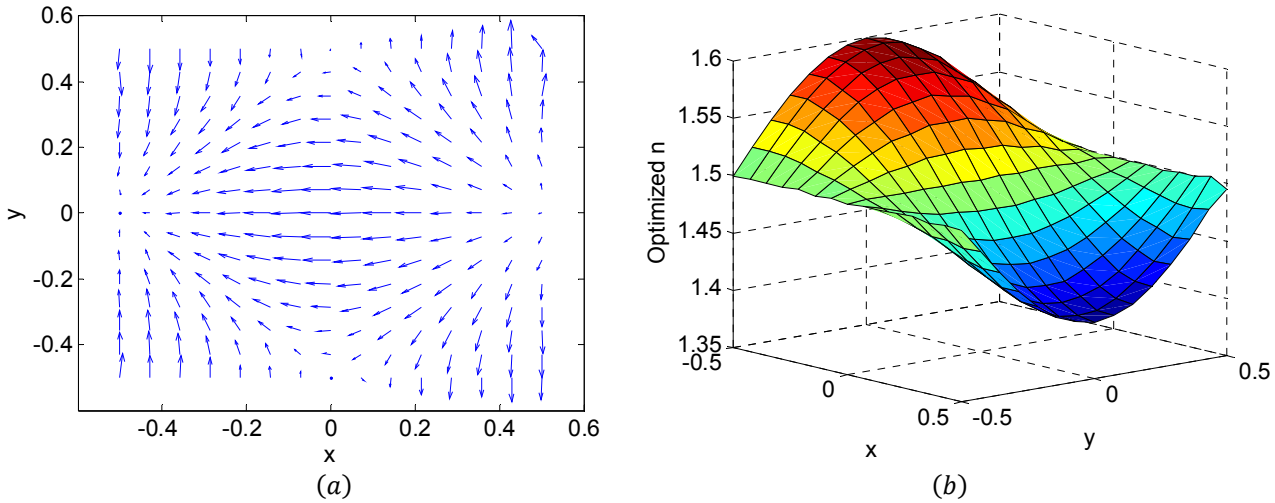

Fig. 4. (a) Index gradient field obtained from system inversion and (b) reconstructed index field after integrating $\nabla w_{l,k}$.

After redefining the test index field in Fig. 3(a) on the same sampling grid, the resulting RMS error in the reconstruction was 7.67×10^{-4} refractive index units, less than 0.5% of the total index range $(n_{max} - n_{min})$. We note that the errors are particularly high in the corner regions of the index field due to the reduced quality of interpolation near the boundaries, resulting in a poor representation of the associated sample points in the discretized deflectometry path integrals.

3.3 Correcting ray trajectories

The beam trajectories inside the medium must obey Eq. (3) for the solution to be consistent with geometrical optics. For this reason, we employed an iterative ray trace procedure to successively refine the beam trajectories. Using the reconstruction in Fig. 4(b) as a starting point, two separate ray traces were performed for each probe beam in the data set. In one instance, we launched the ray with initial conditions associated with its entry point and traced the ray to its exit point; in the other, the ray was launched in reverse with the initial conditions associated with the exit point and was traced to its entry point in similar fashion. A weighted sum of the traced trajectories from both instances was then used to update our tentative approximation to the ray's trajectory in order to ensure that the boundary conditions were not violated in the refined approximation, where the weighting coefficient started at unity at the launch point of the ray trace and decayed to zero as the trace approaches its exit point. The set of refined beam trajectories was then used to recalculate the path integral coefficients in $[S]$ and a more accurate reconstruction of the index field could be obtained by inverting the new system equation. We continued to improve our reconstructions in this manner until agreement was achieved between the ray trace trajectories and the approximate beam trajectories used to obtain the solution.

In order to quantify the inconsistencies in the solution and monitor convergence of the algorithm, it is useful to define an error metric between the assumed trajectories and the traced trajectories; a natural choice is the integrated absolute difference between the two, i.e.,

$$\Delta = \int_a^b |y_{trace}(x) - y_{initial}(x)| dx \ , \tag{9}$$

where $y_{trace}(x)$ is the trajectory obtained from tracing through the computed solution from tracing a ray launched at the entry point of the interrogating ray with the appropriate initial conditions and $y_{initial}(x)$ is the approximation used for trajectory in the computation of $[S]$ prior to system inversion during each iteration of the algorithm. Using our corrective procedure to obtain the beam trajectories inside the index field, we were able to achieve a sufficiently consistent solution after just three successive system inversions. The error metric in Eq. (9) for each probe beam in the data set is shown in Fig. 5, where the probe beams have been sorted in ascending order based on their error metrics in order to prevent coincidental patterns from developing in the plot.

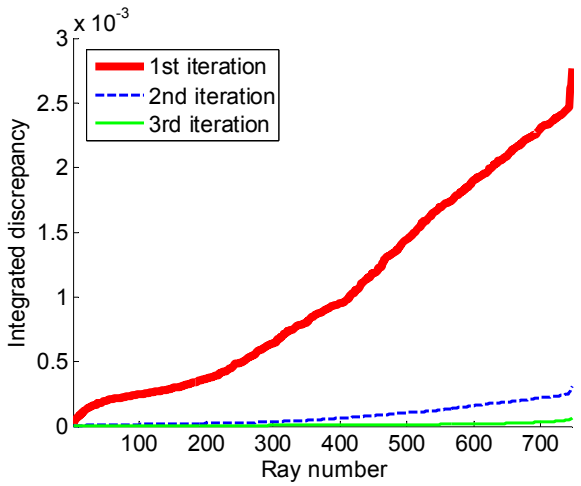

Fig. 5. Progressive improvement in the error metrics evaluated for individual probe beams in the data set after three iterations of refining their trajectories.

The RMS index error for the reconstruction resulting from our corrective procedure did not show a discernible improvement relative to the reconstruction in Fig. 4(b). This suggests that the inversion process is relatively insensitive to small variations in the trajectories associated with individual probe beams. It stands to reason that the coefficients in

$[S]$ remain relatively static when these trajectories are perturbed, at least in the case of slowly varying index fields. Hence, the discrepancies between approximate beam trajectories and those obtained from a ray trace through the actual index distribution are expected to be extremely small.

4. ERROR ANALYSIS

4.1 Quantization error

Much of the reconstruction error observed in Sec. 3 can be attributed to quantization effects. Because the deflectometry data was generated from a numerical ray trace, quantization effects associated with this process introduce random noise to the calculated boundary values of beam location and slope. We took additional measures to reduce this noise source, such as using a higher resolution grid for the test index field during the initial trace and optimizing the step size in Euler's method in implementing the ray trace. Of course, these quantization effects are not present in an actual experiment and the error in the deflectometry data is entirely dictated by measurement accuracy.

Aside from the noise present in the deflectometry data, additional quantization noise is introduced in the discretization of the deflectometry path integral associated with each probe beam. This contribution depends on the quality of interpolation used in obtaining the quantities involved in the path integral, namely, $ds_{l,k}$ and $\hat{n}_{l,k}$ in Eq. (5) under the crude approximation used in Sec. 2, and acts independently of measurement error. Moreover, the numerical integration technique used to discretize Eq. (4) also plays a role. In principle, one can always increase the resolution of the sampling grid to mitigate this source of quantization noise. However, doing so increases the number of unknowns in the system and degrades the numerical conditioning of $[S]$ for the same set of deflectometry data.

4.2 Measurement error

In order to study the impact of measurement error on the reconstructed index field, we introduced white Gaussian noise to the generated deflectometry data (on top of the base-line quantization noise present in the numerical ray trace) prior to system inversion. As a preliminary test, we calculated $[S]$ in the deflectometry system equation based on approximate beam trajectories that fit the noise-free deflectometry data. The deflection values in $\vec{P}$ were subsequently contaminated with artificial Gaussian noise while the coefficients in $[S]$ were held constant. All other simulation parameters were unchanged from the reconstruction in Fig. 4(b). This test allowed us to quantify the base-line inversion sensitivity of the linear system to measurement noise. The result in Fig. 6(a) shows that the RMS index error in the reconstruction increased linearly with the noise level, as one would expect from the direct inversion of any linear system. A separate test is included in the figure and shows the reduction in sensitivity to measurement error through the use of redundant data, where the number of probe beams used to interrogate the index field was increased to 2450.

In a more realistic model, the coefficients in $[S]$ must reflect the changes in the contaminated boundary values as they are generated from approximate trajectories that change with the measured boundary conditions. A subsequent test incorporating changes to both $[S]$ and $\vec{P}$ as a result of the contaminated boundary slope values is shown in Fig. 6(b) and revealed the dependence of system's sensitivity to noise level to be super-linear. This super-linear contribution is due to the path dependence of the coefficients in $[S]$ and becomes negligible for low noise levels. Thus, the overall reconstruction error can be attributed to three primary sources: for extremely small errors in measurement, quantization noise becomes the major contributor; at moderate noise levels, the base-line sensitivity in inverting a linear system is dominant while the super-linear contribution from the path dependence of $[S]$ becomes significant for higher noise levels.

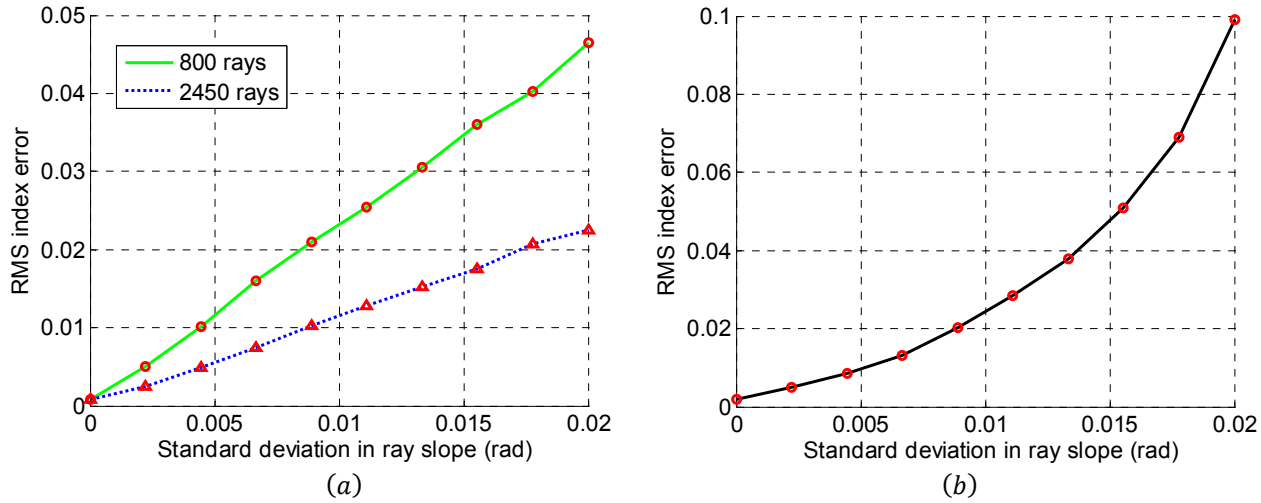

Fig. 6. Index error resulting from contaminated boundary slope values where (a) system coefficients are calculated from noise-free data and (b) system coefficients are recalculated based on the contaminated values.

5. CONCLUSION

We have demonstrated a method for measuring 2-D index fields in rectangular GRIN elements using the boundary values of position and slope for a set of probe laser beams used to interrogate the medium. Using a simplifying assumption that decouples the trajectories of probe beams from the index field, we formulated a linear system description of the inverse problem and developed a mathematical model assuming knowledge of the boundary index values, which were used to obtain the internal boundary slopes for each probe beam. In our model, the beam trajectories were instead approximated from the internal boundary values so that each deflectometry path integral could be expressed as a linear combination of the system's unknowns, i.e., the Cartesian vector components of the index gradient field sampled on a uniform rectangular grid. We solved for these unknowns using a numerical technique suited for inverting sparse and ill-conditioned linear systems. Upon integrating the resulting gradient vector field, we were able to reconstruct the index field to within an arbitrary constant, which was determined through knowledge of the index along the boundaries. Using this approach, we were able to reconstruct a 2-D test index field from deflectometry data generated from a numerical ray trace and achieve RMS index errors below 0.5% of the index range. Taking advantage of the deflectometry system's resilience to slight variations in the ray trajectories, we developed an iterative ray trace procedure to improve the approximated trajectories and refine the mathematical description of the system. The end result enforces the dependence of beam trajectories on the index field so that the optimized solution is consistent with the ray equation of geometrical optics.

In order to assess the sensitivity of reconstruction process to measurement error, we introduced artificial Gaussian noise to the simulated deflectometry data and observed three regimes in the noise level where a particular error mechanism was dominant in contributing to the reconstruction error. The primary error mechanisms include quantization noise, base-line inversion sensitivity and trajectory dependence. We hasten to add that the rectangular geometry of the test index field was chosen to demonstrate our inversion procedure, and the method can be readily adapted to more complex geometries. In addition, the measurement principles can be extended to three-dimensional index distributions. In the future, we plan on exploring methods of reconstructing the index field directly from external beam slopes without knowledge of the boundary index values.

REFERENCES

[1] Moore, D. T., "Gradient-index optics: a review," *Appl. Opt*. **19**, 1035-1038 (1980).

[2] Teichman, J., Holzer, J., Balko, B., Fisher, B. and Buckley, L., "Gradient index optics at DARPA," https://www.ida.org/~/media/Corporate/Files/Publications/IDA_Documents/STD/D-5027-FINAL.pdf IDA Document D-5027, Institute for Defense Analyses (2013).

[3] Sinai, P., "Correction of optical aberrations by neutron irradiation," *Appl. Opt.* **10**, 99-104 (1971).

[4] Pickering, M. A., Taylor, R. L. and Moore, D. T., "Gradient infrared optical material prepared by a chemical vapor deposition process," *Appl. Opt.* **25**, 3364-3372 (1986).

[5] Ohmi, S., Sakai, H., Asahara, Y., Nakayama, S., Yoneda, Y. and Izumitani, T., "Gradient-index rod lens made by a double ion-exchange process," *Appl. Opt.* **27**, 496-499 (1988).

[6] Messerschmidt, B., Possner, T. and Goering, R., "Colorless gradient-index cylindrical lenses with high numerical apertures produced by silver-ion exchange," *Appl. Opt.* **34**, 7825-7830 (1995).

[7] Mohr, R. K., Wilder, J. A., Macedo, P. B. and Gupta, P. K., in *Digest of Topical Meeting on Gradient-index Optical Imaging Systems* (Optical Society of America, Washing, DC 1979), paper WA1.

[8] Wu, S. P., Nihei, E. and Koike, Y., "Large radial graded-index polymer," *Appl. Opt.* **35**, 28-32 (1996).

[9] Liu, J. H., Yang, P. C. and Chiu, Y. H., "Fabrication of high-performance, gradient-refractive-index plastic rods with surfmer-cluster-stabilized nanoparticles," *J. Polym. Sci. A Polym. Chem.* **44**, 5933-5942 (2006).

[10] Liu, J. H. and Chiu, Y. H., "Process equipped with a sloped UV lamp for the fabrication of gradient-refractive-index lenses," *Opt. Lett.* **34**, 1393-1395 (2009).

[11] Urness, A. C., Anderson, K., Ye, C., Wilson, W. L. and Mcleod, R. R., "Arbitrary GRIN component fabrication in optically driven diffusive photopolymers," *Opt. Express* **23**, 264-273 (2015).

[12] G. Beadie, E. Fleet, A. Rosenberg, P. A. Lane, J. S. Shirk, A. R. Kamdar, M. Ponting, A. Hiltner, and E. Baer, "Gradient index polymer optics," *Proc. Of SPIE* **7061**, 706113 (2008).

[13] Ji, S., Yin, K., Mackey, M., Brister, A., Ponting, M. and Baer, E., "Polymeric nanolayered gradient refractive index lenses: technology review and introduction of spherical gradient refractive index ball lenses," *Opt. Eng.* **52** (2013).

[14] Wang C. and Shealy, D. L., "Design of gradient-index lens systems for laser beam reshaping," *Appl. Opt.* **32**, 4763-4769 (1993).

[15] Zahreddine, R. N., Lepkowicz, R. S., Bunch, R. M., Baer, E. and Hiltner, A., "Beam shaping system based on polymer spherical gradient refractive index lenses," *Proc. Of SPIE* **7062**, 706214 (2008).

[16] Lin, D. and Leger, J. R. "Numerical gradient-index design for coherent mode conversion," *Adv. Opt. Technol.* **1**, 195-202 (2012).

[17] Kovalskii, L. V. and Polanskii, V. K., "Application of the prism method for investigating transparent media with a refractive index gradient," *Opt. Spectrosc.* **20**, 408-409 (1966).

[18] Miller, M. and Malisek, V., "Study of the distribution of refractive index by the differential prism method," *Opt. Spectrosc.* **25**, 70-72 (1968).

[19] Oster, G., Wasserman, M. and Zwerling, C., "Theoretical interpretation of moiré patterns," *J. Opt. Soc. Am.* **54**, 169-175 (1964).

[20] Nishijima, Y. and Oster, G., "Moiré patterns: their application to refractive index and refractive index gradient measurements," *J. Opt. Soc. Am.* **54**, 1-5 (1964).

[21] Barnard, A. J. and Ahlborn, B., "Measurement of refractive index gradients by deflection of a laser beam," *Am. J. Phys*. **43**, 573 (1975).

[22] Wiener, O., "Darstellung gekrummter Lichtstrahlen und Verwerthung derselben zur Untersuchung von Diffusion und Warmeleitung," *Ann. Phys. Chem.* **49**,105-149 (1893).

[23] Bodnar, Z. and Ratajczyk, F., "Some remarks concerning optical glass heterogeneity measurement with the help of the autocollimation method," *Appl. Opt.* **4**, 351-354 (1965).

[24] Saunders, J. B., "An interferometer for measuring gradients in both refractive index and thickness of large or small optics," *J. Res. Nat. Bur. Stand.* **63**, 1-4 (1969).

[25] Junginger, H. G. and Van Haeringer, W., "Calculation of three-dimensional refractive-index field using phase integrals," *Opt. Commun.* **5**, 1-4 (1972).

[26] Iwata, K. and Nagata, R., "Calculation of three-dimensional refractive index distribution from interferograms," *J. Opt. Soc. Am.* **60**, 133-135 (1970).
[27] Moore, D. T. and Ryan, D. P., "Measurement of the optical properties of gradient index materials," *J. Opt. Soc. Am.* **68**, 1157-1166 (1978).
[28] Chu, P. L., "Nondestructive measurement of index profile of an optical-fibre preform," *Electron. Lett.* **13**, 736-738 (1977).
[29] Sweeney, D. W. and Vest, C. M., "Reconstruction of three-dimensional refractive index fields from multidirectional interferometric data," *Appl. Opt.* **12**, 2649-2664 (1973).
[30] Yuasa, T., Maksimenko, A., Hashimoto, E., Sugiyama, H., Hyodo, K., Akatsuka, T. and Ando, M., "Hard-x-ray region tomographic reconstruction of refractive-index gradient vector field: imaging principles and comparisons with diffraction-enhanced-imaging-based computed tomography," *Opt. Lett.* **31**, 1818-1820 (2006).
[31] Gasilov, S., Mittone, A., Brun, E., Bravin, A., Grandl, S., Mirone, A. and Coan, P., "Tomographic reconstruction of the refractive index with hard x-rays: an efficient method based on the gradient vector-field approach," *Opt. Express* **22**, 5216-5226 (2014).
[32] Lohmann, A. W., Dorsch, R. G., Mendlovic, D., Zalevsky, Z. and Ferrerira, C., "Space-bandwidth product of optical signals and systems," *J. Opt. Soc. Am. A* **13**, 470-473 (1996).
[33] Elmore, W. C. and Heald, M. A., *Physics of Waves* (Dover, New York, 1985), Chap. 9.
[34] Nishidate, Y., Nagata, T., Morita, S.-Y. and Yamagata, Y., "Ray-tracing method of isotropic inhomogeneous refractive-index media from arbitrary discrete input," *Appl. Opt.* **50**, 5192-5199 (2011).
[35] Paige, C. C. and Saunders, M. A., "LSQR: an algorithm for sparse linear equations and sparse least squares," *AMC Trans. Math. Soft.* **8**, 43-71 (1982).

ACKNOWLEDGEMENTS

The authors would like to thank Jeremy Teichman for his instrumental suggestions and insightful comments on this work. This work was funded by DARPA (contract HQ0034-14-D-0001). The views, opinions, and/or findings contained in this article are those of the authors and should not be interpreted as representing the official views or policies of the Department of Defense or the U.S. Government.